AIP | Journal of Applied Physics

Nonlinear capacitance and electrochemical response of ionic liquid-ionic polymers

Jacob D. Davidson and N. C. Goulbourne

Citation: J. Appl. Phys. 109, 084901 (2011); doi: 10.1063/1.3569709
View online: http://dx.doi.org/10.1063/1.3569709
View Table of Contents: http://jap.aip.org/resource/1/JAPIAU/v109/i8
Published by the AIP Publishing LLC.

Nonlinear capacitance and electrochemical response of ionic liquid-ionic polymers

Jacob D. Davidson and N. C. Goulbourne[a)]
Department of Aerospace Engineering, University of Michigan, Ann Arbor, Michigan 48109, USA

(Received 5 January 2011; accepted 21 February 2011; published online 18 April 2011)

In this paper we present a physics-based model for the electrochemical response of ionic liquid-ionic polymer transducers (IPTs) and show how the mobile ionic liquid ions influence the charging characteristics and actuation performance of a device. It is assumed that a certain fraction of the ionic liquid ions exist as "free," making for a total of 3 mobile ions. This leads to predictions of distinctly different charging characteristics for ionic liquid versus water-based IPTs, since for the latter there is only a single mobile ion. The large ionic liquid ions are modeled by including steric effects in a set of modified Nernst-Planck/Poisson equations, and the resulting system of equations is solved using the method of matched asymptotic expansions (MAE). The inclusion of steric effects allows for a realistic description of boundary layer composition near actuator operating voltages (~1 V). Analytical expressions for the charge transferred and differential capacitance are derived as a function of the fraction of free ionic liquid ions, influence of steric effects in formation of the electric double layer, and applied voltage. It is shown that the presence of free ionic liquid ions tends to increase the overall amount of charge transferred, and also leads to a nonmonotonic capacitance-voltage curve. We suggest that these results could be used to experimentally identify the extent of free ionic liquid ion movement and to test the validity of the assumptions made in the underlying theory. A comparison with numerical results shows that while the MAE solution procedure gives valid results for capacitance and charge transferred, it cannot predict the dynamic response due to the presence of multiple time scales in the current decay. This is in contrast to previous results in analyzing water-based IPTs, where the MAE solution is in good agreement with numerical results at all times and applied voltages due to the presence of only a single mobile ion. By examining the structure of the electric double layer in the ionic liquid IPT, it is shown that although the additional mobile ions lead to more charge transferred, they likely do not increase the bending moment generated by a cantilevered IPT because of the increase in symmetry in boundary layer charge density profiles. These results are in good qualitative agreement with recent experiments. © *2011 American Institute of Physics*. [doi:10.1063/1.3569709]

I. INTRODUCTION

Ionic polymer transducers (IPTs) are sensors and actuators which operate through a coupling of molecular-scale chemical, electrical, and mechanical interactions. These transducers consist of an ion-exchange membrane placed in a certain cation form (typically Li^+ or Na^+), solvated with a polar solvent, and electroded on both sides. When a DC voltage (1–5 V) is applied to the faces of an IPT in a cantilever configuration, the transducer will bend toward the anode as shown in Fig. 1. Conversely, a voltage will be generated by an IPT when a mechanical deformation is imposed.

Recent work has specifically focused on using ionic liquids in IPTs.[1–9] The environmental and electrochemical stability of an ionic liquid in actuator systems allows for lasting device performance in free-air usage and at higher applied potentials.[10,11] However, despite the advantages of using ionic liquids, the charge transport and actuation mechanisms in these devices are not well understood; a model does not currently exist that explains the observed differences in charging and actuation characteristics for IPTs with different ionic liquids, and for ionic liquid IPTs in comparison with water-based IPTs. This work represents the first time a physics-based approach has been taken in modeling the unique actuation and charging characteristics of ionic liquid IPTs.

In an ionic liquid IPT, the charging characteristics are distinctly different from a water-based IPT due to the presence of the ions of the ionic liquid, which make for a total of 3 mobile ionic species. The presence of multiple mobile ionic species in ionic liquid IPTs has been noted in recent experimental investigations.[6–8] In our previous work, we applied Nernst-Planck/Poisson theory to form an electrochemical model of charge transport in ionic liquid IPTs by considering 3 mobile ionic species, and obtained numerical solutions using the finite element method to analyze boundary layer charge dynamics.[12] However, these solutions were limited to low applied voltages due to the treatment of the ions as point charges. At typical transducer operating voltages, steric effects between the ions of the ionic liquids become important as these large ions pack into the electric double layer. The influence of steric effects on the structure of the electric double layer has been modeled in electrolyte solutions at high concentrations and large applied voltages

a)Electronic mail: ngbourne@umich.edu.

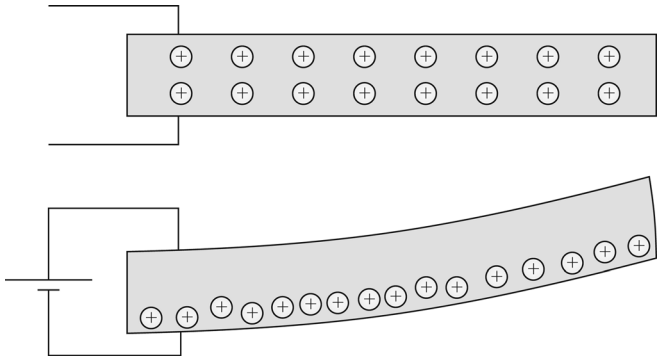

FIG. 1. An IPT will bend toward the anode when a voltage is applied due to cation and solvent movement.

(see, for example, Refs. 13–23), and has recently been modeled in neat ionic liquids.[24–27] Here, we use the so-called modified Nernst-Planck/Poisson (MNPP) equations to model the electrochemical behavior of the large ionic liquid ions. The mathematical treatment is similar to that presented by Kilic *et al.*[21,22] We show how the electrochemical response of an ionic liquid IPT depends on the movement of the ionic liquid ions, and compare this with corresponding results for water-based IPTs. Analytical expressions for the charge transferred and differential capacitance are derived using the method of matched asymptotic expansions (MAE), and the boundary layer concentration profiles for the mobile ions are computed. The MAE solution procedure greatly simplifies the analysis and computational cost in comparison to a full numerical solution and allows for analytical expressions for charge transferred and capacitance to be obtained. The presence of mobile ionic liquid ions will tend to increase the total amount of charge transferred when a voltage is applied, and also leads to a nonmonotonic capacitance-voltage relation. The current response obtained from the MAE solution procedure is compared to numerical results at low applied voltages, thus demonstrating when the implicit assumption of linear dynamics introduced by using the MAE solution procedure is a good approximation of the charging dynamics. When there is a single mobile ionic species, the MAE solution is a good description of charging dynamics at all times and applied voltages, but when there are multiple mobile ions, the MAE solution becomes a poor description of charging dynamics due to the presence of multiple time scales in the coupled response. These results are discussed along with explanations regarding the performance characteristics of ionic liquid IPTs as actuators and electrochemical supercapacitors and suggestions for future device development.

The paper is organized as follows. In Sec. II we assemble the governing equations for the transient charging response of an ionic liquid IPT. In Sec. III the resulting system of equations is solved using the method of matched asymptotic expansions. The solution is applied to determine the charge transferred and capacitance of the IPT as a function of the applied voltage in Sec. IV. The dynamic charging response from the matched asymptotic expansion is compared to numerical results in Sec. V, and the charge density and individual ionic concentration profiles are computed numerically in Sec. VI. These results are discussed in Sec. VII in comparison to a water-based IPT, and the implications toward device performance are noted. The conclusions are summarized in Sec. VIII.

II. MODEL DEVELOPMENT

When a voltage is applied to the faces of an IPT, the mobile ions in the ionomer will move to screen the applied field. The movement of ions causes the formation of thin layers near each electrode that have an excess or a depletion of charge. These layers, referred to as boundary layers, are the "active regions" during actuation. Electrostatic interactions between the ions cause pressures to develop in the boundary layers, and the resulting pressure gradient causes the movement of solvent molecules. The boundary layers will either expand or contract as the solvent molecules move to neutralize the pressure gradient, causing an elastic deformation of the polymer backbone material. Equilibrium will consist of a balance between electrostatic interactions, migration and diffusion potentials, and the resulting elastic stress from boundary layer expansion or contraction. It is found that the cathode boundary layer undergoes a larger expansion than the anode boundary layer, and thus an IPT in a cantilever configuration will bend toward the anode as shown in Fig. 1. For more details on IPT actuation mechanisms, see, for example, Refs. 28 and 29 as well as our previous work.[12]

It is well known that the actuation performance of an IPT is directly related to its capacitance; see, for example Akle *et al.*[30] NPP theory has been widely used as a standard model in describing electrochemical migration of the ions of an electrolyte solution under an applied potential,[23,31–34] and the charging characteristics of IPTs are commonly modeled by applying the Nernst-Planck/Poisson (NPP) system of equations and taking the neutralizing counter-cation to be the only mobile ionic species. An analytical solution for the equilibrium charge distribution considering a single mobile ionic species in an IPT was given by Nemat-Nasser,[29] and numerical solutions featuring a coupling to the actuation response were obtained by Wallmersperger *et al.*[35–37] and Leo *et al.*[38] Porfiri[39] showed that the capacitance of an IPT is a decreasing function of the applied voltage, and incorporated these results into an actuation model which shows the influence of electrode structure on charge transferred and actuation performance.[40] Aureli *et al.*[41] demonstrated how rough electrodes lead to a large increase in the capacitance of the IPT due to the large microscopic surface area; their model uses a local value of the electric permittivity (bounds for IPT permittivity are given by Porfiri[42]) and incorporates effects of electrode roughness due to the fractal-like electrode structure commonly observed in IPTs. Chen *et al.*[43] used equilibrium numerical solutions of the NPP equations to form a nonlinear circuit model of an IPT. Other research has also focused on equivalent circuit representations of IPTs.[44–49] Farinholt and Leo[48] include a theoretical and experimental analysis of the impedance response of IPTs in the frequency domain.

Here, we use NPP theory for the counter-cation and the so-called MNPP equations for the ionic liquid ions. The

MNPP equations were first derived by Bikerman[13] and have since been reformulated by a number of authors.[14–20] The equations can be derived using a lattice-gas model which includes steric effects by accounting for the finite size of the ions in the entropic contribution to the free energy. For a complete review of the theoretical developments describing steric effects in electrolytes, see Bazant *et al.*[23] Here, we begin with the electrochemical potential for each ionic species; more details on the derivation of the MNPP equations, including the free energy expressions for the system, can be found elsewhere.[13–24] Letting the indices 1, 2, and 3 correspond to the counter-cation, ionic liquid anion, and ionic liquid cation, respectively, the electrochemical potentials of each ionic species are

$$\mu_1 = F\Phi + RT\ln C_1, \tag{1a}$$

$$\mu_2 = -F\Phi + RT\ln\frac{C_2}{C_{\max} - C_2 - C_3}, \tag{1b}$$

$$\mu_3 = F\Phi + RT\ln\frac{C_3}{C_{\max} - C_2 - C_3}, \tag{1c}$$

where Φ is the electric potential, $C_{\max}$ is the maximum concentration of the ionic liquid ions, and R, T, and F are the universal gas constant, temperature in Kelvin, and Faraday's constant, respectively. For simplicity, we assume that the sizes of the ionic liquid ions are equal so that $C_{\max}$ is the same for both the anion and cation. It is important to note the difference in Eq. (1a) with Eqs. (1b) and (1c). In Eq. (1a), the term $RT\ln C_1$ is obtained by using Boltzmann's equation and applying Maxwell-Boltzmann statistics in the typical limit where the number of possible states is much larger than the number of particles. Eqs. (1b) and (1c) contain the same term, respectively, for the different ions, but have the additional term $-RT\ln(C_{\max} - C_2 - C_3)$. As $C_2 + C_3 \to C_{\max}$, this term tends to positive infinity, meaning that the energy required to further increase the concentration of either ionic liquid ion becomes infinite. This leads to a maximum in ionic concentration.

To be strict, steric effects should also be included for the counter-cation, since the same reasoning would certainly apply in imposing a finite maximum concentration. The inclusion of steric effects in describing a single mobile ionic species in an IPT was recently addressed by Porfiri.[40] Here, since the counter-cation is generally much smaller than the ionic liquid ions, we omit steric effects for the counter-cation in order to simplify the analysis and focus on the essential mechanisms caused by the movement of the large ionic liquid ions.

Using a linear diffusion model (Fick's law of diffusion), the flux of each ionic species is

$$J_i = -\frac{D_i C_i}{RT}\frac{\partial \mu_i}{\partial X}, \tag{2}$$

where D_i are the individual ionic diffusion coefficients. Symmetry along the length and width of the IPT is presumed to reduce the problem to the through-thickness direction X as shown in Fig. 2. The continuity equation for each ionic species is

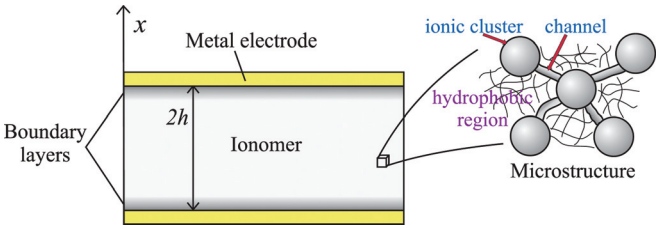

FIG. 2. (Color online) A diagram of the system for modeling ion transport, showing the through-thickness x direction and the microstructure of Nafion.

$$\frac{\partial C_i}{\partial \tau} + \frac{\partial J_i}{\partial X} = 0, \tag{3}$$

where τ is the temporal variable. From elementary electrostatics, the Poisson equation for the system is

$$\frac{\partial^2 \Phi}{\partial X^2} = -\frac{F}{\varepsilon}(C_1 - C_2 + C_3 - C_0), \tag{4}$$

where ε is the local permittivity of the IPT and C_0 is the concentration of the fixed anionic groups, both of which are assumed to be constant. The governing equations for the ionic liquid IPT system consist of Eq. (4) along with the result of inserting Eqs. (1) and (2) into Eq. (3).

To proceed, we first nondimensionalize using the following definitions:

$$\varphi = \Phi\frac{F}{RT}, \qquad c_i = \frac{C_i}{C_i^0}, \qquad x = \frac{X}{h}, \qquad t = \frac{\tau}{\tau_c}. \tag{5}$$

The characteristic time scale for the problem is chosen following Bazant *et al.*[50] and Kilic *et al.*[21,22] as well as our previous work[9,51] to be

$$\tau_c = \frac{\lambda h}{D_1}, \qquad \lambda = \left(\frac{\varepsilon RT}{C_0 F^2}\right)^{1/2}, \tag{6}$$

where λ is the Debye length.

In an ionic liquid IPT, it is not known if all, some, or none of the ions of the ionic liquid exist as "free" ions, able to selectively move under the applied field. In contrast to a neat ionic liquid, specific interactions with the ionomer are likely to change the state of ionic liquid ions swollen in an IPT. Here, we build on the description of charge transport in an ionic liquid IPT given by Bennett,[1,52] who took the counter-cation to be the only mobile charge carrier, and consider how the introduction of mobile ionic liquid ions influences the actuation and charging characteristics. This is also the same approach taken in our previous work.[12] Since the fraction of free ionic liquid ions is not known, we set $C_2^0 = C_3^0 = \alpha C_1^0$, where $C_1^0 = C_0$ and α represents the fraction of free ionic liquid ions versus mobile counter-cations. Additionally, we introduce the parameter β to represent the relative diffusion coefficient of the ionic liquid ions to the counter-cations, set equal for simplicity: $D_2 = D_3 = \beta D_1$. Note that α and β are likely different for the ionic liquid anion and cation, e.g., if it was seen that ionic liquid cations

replace counter-cations than there would be more free ionic liquid cations than anions. For this case, using α_- and α_+ for the ionic liquid anion and cation instead of $\alpha_- = \alpha_+ = \alpha$ would be a straightforward extension of the current model. Here we retain single values of α and β for the ionic liquid anion and cation for simplicity in analyzing the dominant charge transfer response. Now, also defining $\delta = \lambda/h \ll 1$, the governing equations become

$$\frac{\partial c_1}{\partial t} + \delta \frac{\partial j_1}{\partial x} = 0, \tag{7a}$$

$$\frac{\partial c_2}{\partial t} + \delta\beta \frac{\partial j_2}{\partial x} = 0, \tag{7b}$$

$$\frac{\partial c_3}{\partial t} + \delta\beta \frac{\partial j_3}{\partial x} = 0, \tag{7c}$$

$$\delta^2 \frac{\partial^2 \phi}{\partial x^2} = -c_1 + \alpha c_2 - \alpha c_3 + 1, \tag{7d}$$

where $j_i = J_i h/(D_i C_i^0)$ is the nondimensional flux. Taking the electrodes to be blocking, the boundary and initial conditions are written in nondimensional form as

$$c_i(x, 0) = 1, \tag{8a}$$

$$j_i(\pm 1, t) = 0, \tag{8b}$$

$$\phi(\pm 1, t) = \pm \frac{v_0}{2}, \tag{8c}$$

where v_0 is the nondimensional applied voltage. Following the same notational convention, we later use V_0 to refer to the dimensional applied voltage.

III. MATCHED ASYMPTOTIC EXPANSIONS

In this section, the method of matched asymptotic expansions (MAE) is applied to find an approximate solution to Eq. (7) with boundary and initial conditions in Eq. (8). The basic approach consists of nondimensionalizing the governing equations, obtaining an outer solution valid in the bulk region, changing coordinates to obtain an inner solution valid in the boundary layers, enforcing matching conditions between the two solutions in the limit of thin boundary layers, and using these conditions to obtain an approximate solution to the governing equations. This yields a set of analytical expressions for the charge transferred and differential capacitance as a function of the applied voltage. The derived first order ODE's are then solved numerically to obtain current and the ionic concentration profiles.

As an alternative to using the MAE solution procedure, Eqs. (7) and (8) could be directly solved numerically. However, especially due to the nonlinearities from the inclusion of steric effects, as well as the thinness of the boundary layers, a full numerical solution would require significant computational effort. Since the MAE solution procedure leads to analytical results or relatively simple ODE's to solve, it has the distinct advantage of being able to easily show how the fraction of free ionic liquid ions (α), relative diffusion coefficient of the ionic liquid ions (β), influence of steric effects on the electric layer [later defined in Eq. (15) as κ], and magnitude of the applied voltage affect the leading order charging and actuation characteristics of the transducer.

The method of matched asymptotic expansions has been previously applied to analyze electrochemical systems, [21,22,50,53–55] and also to analyze the charging characteristics of IPTs with a single mobile ionic species.[39,40] The analysis here has similarities to that of Porfiri[39,40] and Kilic,[21,22] but with a different electrochemical system under consideration. In Refs. 39 and 40, a single mobile species was assumed in modeling the IPT. In Refs. 21 and 22, a symmetric binary electrolyte was considered. For the ionic liquid IPT system, we now have 3 mobile ionic species: the counter-cation and the (assumed) symmetric ionic liquid ions, with an unknown free concentration represented by α. To this end, when $\alpha = 0$ our results reduce to those in Ref. 39, and if the counter-cation and fixed anionic groups are omitted, become identical to those in Refs. 21 and 22. However, the consideration of 3 mobile ionic species in an ionic liquid IPT leads to distinct differences in the underlying physical mechanisms and the associated observable charging characteristics in comparison with the results in Refs. 21, 22, 39.

A. Inner and outer expansions

For the outer, or bulk, region, denoted by the bar accent, the expansion is of the form

$$c_i = \bar{c}_i(x, t) = \bar{c}_i^{(0)} + \delta \bar{c}_i^{(1)} + \ldots$$

Using this in Eq. (7) along with the boundary conditions in Eq. (8) and equating terms with like powers of δ yields the leading order solution of the system of PDE's:

$$\bar{\varphi}^{(0)}(x, t) = \frac{A(t)}{2} x + B(t), \tag{9a}$$

$$\bar{c}_i^{(0)}(x, t) = 1. \tag{9b}$$

The coefficients $A(t)$ and $B(t)$ may be functions of time, since $\bar{\varphi}^{(0)}$ was obtained by only integrating with respect to x. At an equilibrium time t_e the potential is constant in the bulk region and thus $A(t_e)$ must equal 0. Therefore, $B(t_e)$ is identified as the bulk potential "offset," which is zero for a symmetric electrolyte. For the IPT system, the presence of fixed anionic groups leads to a highly asymmetric charge distribution, and therefore $B(t_e) \neq 0$.

To examine the boundary layers, we first need to make a coordinate transformation to the inner or "stretching" coordinate, defined as $\eta^{\pm} = (1 \mp x)/\delta$. The cathode boundary layer is thus modeled with η^-, and the anode boundary layer with η^+. The inner expansion, denoted by the hat accents, is of the form

$$c_i = \hat{c}_i^{\pm}(\eta^{\pm}, t) = \hat{c}_i^{\pm(0)} + \delta \hat{c}_i^{\pm(1)} + \ldots$$

Note that there are now two expressions for potential and concentration, e.g., $\hat{\varphi}^-$ and $\hat{\varphi}^+$, which correspond to the boundary layer coordinates η^- and η^+, respectively. For ease of notation, the $\pm$ designation will be left off and only specified where necessary to differentiate between the two

solutions. This change of variables removes the singular perturbation in the Poisson equation, and the governing equations now become

$$\delta\frac{\partial\hat{c}_1}{\partial t}+\frac{\partial\hat{j}_1}{\partial\eta}=0, \tag{10a}$$

$$\delta\frac{\partial\hat{c}_2}{\partial t}+\beta\frac{\partial\hat{j}_2}{\partial\eta}=0, \tag{10b}$$

$$\delta\frac{\partial\hat{c}_3}{\partial t}+\beta\frac{\partial\hat{j}_3}{\partial\eta}=0, \tag{10c}$$

$$\frac{\partial^2\hat{\phi}}{\partial\eta^2}=-\hat{c}_1+\alpha\hat{c}_2-\alpha\hat{c}_3+1. \tag{10d}$$

The fraction of free ionic liquid ions to mobile counter-cations, α, is contained in the nondimensional form of the Poisson equation [Eq. (10d)].

Matching between the inner and outer solutions is enforced in the limit of thin boundary layers, e.g.,

$$\lim_{\delta\to0}\hat{c}_i(\eta)=\lim_{\delta\to0}\bar{c}_i(x).$$

Using the definition of $\eta^{\pm}$, this is equivalently expressed as

$$\lim_{\eta^{\pm}\to\infty}\hat{\varphi}^{\pm}(\eta^{\pm})=\lim_{x\to\pm1}\bar{\varphi}(x)=\pm\frac{A(t)}{2}+B(t), \tag{11a}$$

$$\lim_{\eta^{\pm}\to\infty}\hat{c}_i{}^{\pm}(\eta^{\pm})=\lim_{x\to\pm1}\bar{c}_i(x)=1, \tag{11b}$$

where Eq. (9) is also used. These are known as the van Dyke matching conditions between the inner and outer solutions.[21]

B. Leading order solution to inner expansion

Eq. (10) consists of 4 coupled equations for the 4 unknown variables $\hat{\varphi}$ and $\hat{c}_i$. However, since at leading order Eq. (10) contains no terms with a time dependence, it is taken that the boundary layers are in a state of quasiequilibrium with the bulk region. This occurs because the Debye time, $\tau_D=\lambda^2/D_1$, is the characteristic time scale for local ion movement into the boundary layers, and this quantity is much smaller than the charging time scale: $\tau_D\ll\tau_c$.[21,50] We can therefore use the equilibrium condition of constant chemical potential to obtain a leading order relationship between ionic concentration and potential in each boundary layer:

$$\hat{\mu}_i(\hat{c}_i^{(0)},\,\hat{\varphi}^{(0)})=\hat{\mu}_i(1,\,\hat{\varphi}_B), \tag{12}$$

where $\hat{\varphi}^{(0)}$ refers to leading order potential in the diffuse region and $\hat{\varphi}_B$ is potential in the bulk region, where the ionic concentrations at leading order are 1 according to Eq. (9b). The effective bulk potential for each boundary layer is the potential as the inner coordinate goes to infinity, i.e., $\hat{\varphi}_B^{\pm}=\lim_{\eta^{\pm}\to\infty}\hat{\varphi}^{\pm}$, which is defined using the matching conditions in Eq. (11). The difference between the potential at a point in the diffuse layer and the bulk potential is called the zeta potential, and this is defined for each inner coordinate as

$$\hat{z}^{\pm}=\hat{\varphi}^{\pm}-\hat{\varphi}_B^{\pm}. \tag{13}$$

Now, using Eq. (1) for the electrochemical potentials of the ions, Eqs. (12) and (13) lead to the following leading order expressions for the ionic concentrations as a function of zeta potential:

$$\hat{c}_1^{(0)}=e^{-\hat{z}^{(0)}}, \tag{14a}$$

$$\hat{c}_2^{(0)}=\frac{e^{\hat{z}^{(0)}}}{1-\kappa+\kappa\cosh\hat{z}^{(0)}}, \tag{14b}$$

$$\hat{c}_3^{(0)}=\frac{e^{-\hat{z}^{(0)}}}{1-\kappa+\kappa\cosh\hat{z}^{(0)}}, \tag{14c}$$

where

$$\kappa=\frac{2}{c_{\max}} \tag{15}$$

is the ion-packing parameter. $\kappa\to0$ represents an infinite maximum concentration, i.e., treating the ions as point charges. In an ionic liquid, the ions form a latticelike structure which also has "holes" that fluctuate due to Brownian motion.[32] Because of the holes, the maximum concentration, say, the cations reach can be greater than twice its initial concentration (considering a neat ionic liquid and assuming both ions have equal size).[56] For an ionic liquid IPT, the correct value to choose for κ is unclear, since not all of the ionic liquid ions are free, and because the boundary layers in an IPT will expand as ions and solvent move in. For these reasons, a smaller value of κ than that for a neat ionic liquid is likely to be appropriate. We discuss reasonable values of κ for an ionic liquid IPT in Sec. IV.

Equation (14a) is the typical Boltzmann distribution, while Eqs. (14b) and (14c) include the effects of lattice saturation and represent modified Boltzmann distributions. Substituting Eq. (14) into Eq. (10d) yields the leading order modified Poisson-Boltzmann equation for the system:

$$\frac{\partial^2\hat{z}^{(0)}}{\partial\eta^2}=\frac{2\alpha\sinh\hat{z}^{(0)}}{1-\kappa+\kappa\cosh\hat{z}^{(0)}}-e^{-\hat{z}^{(0)}}+1. \tag{16}$$

This equation is integrated to obtain

$$\frac{1}{2}\left(\frac{\partial\hat{z}^{(0)}}{\partial\eta}\right)^2=\frac{2\alpha}{\kappa}\ln\left(1-\kappa+\kappa\cosh\hat{z}^{(0)}\right)+e^{-\hat{z}^{(0)}}+\hat{z}^{(0)}-1, \tag{17}$$

where the constant of integration is determined using the condition $\lim_{\eta\to\infty}\hat{z}=0$ to be -1.[39] We now note that since the leading order system of equations for the inner expansion does not have a time dependence, conservation of charge must be explicitly enforced.[39] This is because the continuity equation is not included in obtaining the leading order solution, and there is no remaining consideration in the equations to prevent charge from being created or destroyed. A satisfactory condition is obtained by applying Gauss's law and transforming to the inner coordinates:

$$\left.\frac{d\hat{\varphi}^{+(0)}}{d\eta^{+}}\right|_{0} = -\left.\frac{d\hat{\varphi}^{-(0)}}{d\eta^{-}}\right|_{0}. \tag{18}$$

Now, take Eq. (17) at each boundary, $\eta^{-} = 0$ and $\eta^{+} = 0$, subtract the resulting two equations, and apply the charge conservation condition in Eq. (18) to simplify. To simplify the notation, let $\xi^{\pm}$ represent the leading order inner solution for the zeta potential at each electrode, i.e., $\xi^{\pm} = \hat{z}^{\pm(0)}(0)$. Using the boundary conditions in Eq. (8) transformed to η-coordinates, the bulk potential for the inner solution defined from the matching conditions in Eq. (11), and the definition of the zeta potential in Eq. (13), we obtain a simple relationship for y, the total potential drop over the boundary layers:

$$y = \xi^{+} - \xi^{-} = v_0 - A(t). \tag{19}$$

At equilibrium, $A = 0$ and y is equal to the applied voltage. Now the governing equation for $\xi^{\pm}$ as a function of y can be defined, which is written here using ξ^{+}:

$$G(\xi^{+}, y, \alpha) \equiv \frac{2\alpha}{\kappa}\ln\left(\frac{1-\kappa+\kappa\cosh\xi^{+}}{1-\kappa+\kappa\cosh(\xi^{+}-y)}\right) + e^{-\xi^{+}}(1-e^{y}) + y = 0 \tag{20}$$

This equation can be solved numerically to determine $\xi^{\pm}(y)$. However, when α is small, an approximate analytical solution of Eq. (20) solution can be used to derive analytical expressions for charge transferred and differential capacitance as functions of the applied voltage. We derive this approximate solution here to use in Sec. IV. In Sec. V and VI a numerical solution of Eq. (20) is used to examine the dynamic response and the boundary layer ionic concentration profiles.

For small α, we seek a solution to Eq. (20) of the form

$$\xi^{+} = \xi_0^{+} + \alpha\xi_1^{+} + \ldots.$$

The first two terms in this expansion are then determined by using the Taylor series expansion of $G(\xi^{+}, y, \alpha)$ about $\alpha = 0$, i.e., by solving

$$G(\xi_0^{+}, y, 0) = 0, \tag{21a}$$

$$\left.\frac{\partial G(\xi_1^{+}, y, \alpha)}{\partial\alpha}\right|_{\alpha=0} = 0. \tag{21b}$$

Eq. (21a) is solved for ξ_0^{+} and Eq. (21b) is solved for ξ_1^{+}. The series expansion of $G(\xi^{+}, y, \alpha)$ about $\alpha = 0$ is terminal and contains only two terms. Solving Eq. (21) yields the leading order inner solution for the zeta potential at each electrode:

$$\xi^{+} = \ln\left(\frac{e^{y}-1}{y}\right) + \alpha\frac{y}{2}, \tag{22a}$$

$$\xi^{-} = \ln\left(\frac{e^{y}-1}{y}\right) - \alpha\frac{y}{2} - y. \tag{22b}$$

Because a series expansion was used to obtain Eq. (22), it is seen that Eq. (19) is not satisfied, i.e., $\xi^{+} - \xi^{-} \neq y$. This condition can be enforced by setting

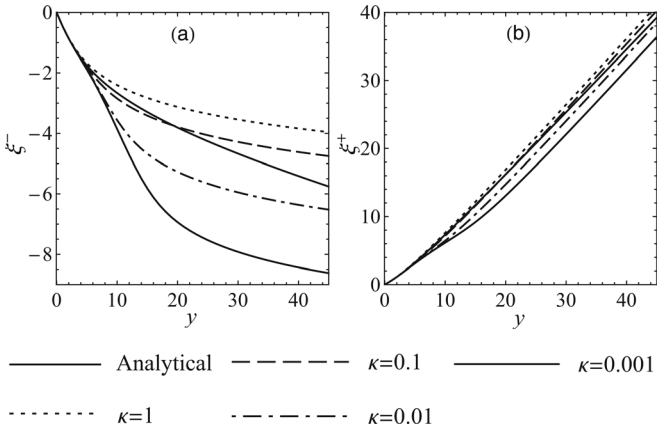

FIG. 3. The inner zeta potential as a function of the total potential drop over the boundary layers (y) with a free ionic liquid fraction of $\alpha = 0.1$ at (a) the cathode (ξ^{-}) and (b) the anode (ξ^{+}), showing the analytical solution in Eq. (22) compared with results obtained by numerically solving Eq. (20) for different values of κ.

$$y = \frac{v_0 - A(t)}{\alpha + 1} \tag{23}$$

when Eq. (22) is used. The leading order zeta potentials at the cathode, ξ^{-}, and at the anode, ξ^{+}, are plotted in Fig. 3 for $\alpha = 0.1$. The approximate result in Eq. (22) is compared with numerical solutions of Eq. (20). Although Eq. (22) does not depend on κ, the numerical solution does; as shown in Fig. 3, the difference is larger for ξ^{-} than for ξ^{+} since ξ^{-} is smaller in magnitude. This means that although in principle either value of the zeta potential should yield the same result in calculating charge transferred and capacitance, the approximate solution in Eq. (22) leads to different results for ξ^{-} versus ξ^{+}. Since ξ^{+} has a smaller relative difference from the numerical solution, however, it is seen to lead to a better correlation with results for charge transferred and capacitance obtained by using a numerical solution of Eq. (20). We therefore use ξ^{+} in the next section to obtain analytical expressions for these quantities and to examine how they depend on α, κ, and y.

IV. CAPACITANCE AND CHARGE TRANSFERRED

Using Gauss's law, the charge per unit surface area stored at either electrode in the limit of thin boundary layers is expressed in nondimensional form using the inner coordinates as

$$q^{\pm} = \frac{\lambda F}{\varepsilon RT}Q^{\pm} = \pm\left.\frac{\partial\hat{\varphi}^{\pm(0)}}{\partial\eta^{\pm}}\right|_{\eta^{\pm}=0} = \pm\frac{\partial\xi^{\pm}}{\partial\eta^{\pm}}, \tag{24}$$

where q refers to nondimensional and Q to dimensional charge transferred. This equation was already used to express the condition for conservation of charge in Eq. (18). From Eq. (24) it is clear that smaller boundary layers lead to larger amounts of charge transferred. This result seems counter-intuitive at first, however, it is well known in interfacial electrochemistry and follows from the flux equations and the definition of the Debye length. As the concentration of an electrolyte increases, more charge will be held in the electric

double layer in response to an applied voltage. From Eq. (6), the size of the double layer varies inversely with the initial concentration, and therefore charge transferred varies inversely with the size of the boundary layers. For an ionic liquid, charge transferred still varies inversely with the size of the boundary layers for a given applied potential, but the relationship will be affected by steric effects which cause the boundary layer size to increase with the applied potential. Using the point charge approximation in classic NPP theory, the boundary layer size is independent of the applied potential. From the definition of the nondimensional charge transferred in Eq. (24), it also follows that the total charge transferred is independent of the polymer thickness $2h$. This result is also well known in analyzing the electric double layer.[34]

The charge transferred is now obtained by inserting either ξ^+ or α from Eq. (22) into Eq. (17), and then using the results in Eq. (24). Taking charge transferred to be positive, i.e., $q = |q^-| = |q^+|$, and using ξ^+ this yields

$$q = \sqrt{2}\left[e^{-\xi^+} + \xi^+ - 1 + + \frac{2\alpha}{\kappa}\ln\left(1 - \kappa + \kappa\cosh\xi^+\right)\right]^{1/2}. \tag{25}$$

ξ^+ is used in Eq. (25) [and in Eq. (26)] because of its better relative agreement with the numerical solution, a comparison of which was shown in Fig. 3. We showed in our previous work[57] that the analytical expressions for charge transferred and differential capacitance [Eqs. (25) and (26)], which use the approximate solution of ξ^+ in Eq. (22a), show a good correlation with results obtained by numerically solving for ξ^+ when the fraction of free ionic liquid ions is small and steric effects are included.

The specific differential capacitance of the IPT is the change in charge transferred with respect to a change in the applied voltage. However, the applied voltage referred to here is the potential difference which functions to move charge. This corresponds to the total potential drop across the boundary layers, y. Therefore, the specific differential capacitance is

$$\omega = \frac{\lambda}{\varepsilon}\Omega = \frac{\partial q}{\partial y}$$

where ω is nondimensional and Ω is dimensional capacitance. Using Eq. (25), this is evaluated to be

$$\omega = \frac{1}{q}\left(1 - e^{-\xi^+} + \frac{2\alpha\sinh\xi^+}{1 - \kappa + \kappa\cosh\xi^+}\right)\left(\frac{e^y}{e^y - 1} - \frac{1}{y} + \frac{\alpha}{2}\right). \tag{26}$$

Eqs. (25) and (26) give the charge transferred and capacitance of the ionic liquid IPT as a function of the total potential drop across the boundary layers (y) and the modeling parameters α and κ, which represent the fraction of free ionic liquid ions and the influence of steric effects, respectively. Figure 4 shows the charge transferred and Fig. 5 the differential capacitance, plotted as functions of the total boundary layer potential drop. In Figs. 4(a) and 5(a), $\alpha = 0.1$ and κ is varied, and in Figs. 4(b) and 5(b), $\kappa = 0.1$ and α is varied.

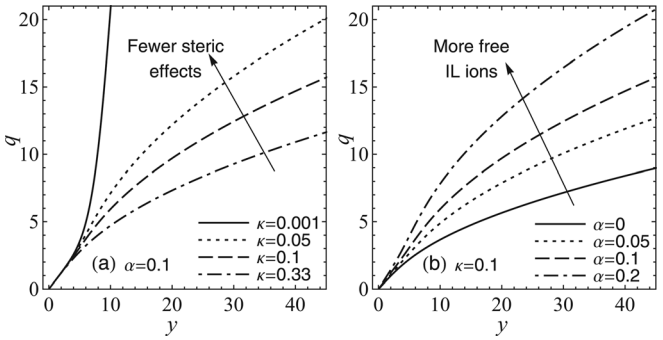

FIG. 4. Nondimensional charge transferred for (a) a free ionic liquid fraction of $\alpha = 0.1$ with different values of the ionic liquid ion packing parameter, κ, and (b) $\kappa = 0.1$ and different values of α.

For reasonable values of α and κ we estimate $\alpha = 0.1$ and $\kappa = 0.1$. In an ionic liquid IPT actuator, the number of ionic liquid ions per sulfonate group is ~ 2 (the discussion and calculations behind this estimate are in Ref. 12). This means that the ratio of free ionic liquid ions to the total amount of ionic liquid ions is $\sim\alpha/2$. Because of this, the maximum concentration of free ionic liquid ions relative to their initial concentration may be better represented as $(2/\alpha)(2/\kappa)$ instead of $2/\kappa$. Therefore, $\kappa \sim 1$ is an unrealistic parameter choice for the ionic liquid IPT system when $\alpha \ll 1$. For simplicity, we choose $\alpha = \kappa$ for reasonable parameter values, and note that we may even have $\kappa < \alpha$ for the system. The concentration of free ionic liquid ions is also likely to depend on the magnitude of the applied voltage and may vary in time when a voltage is applied;[12] this effect is ignored in the current treatment.

Figure 4 shows that the overall amount of charge transferred increases when α increases, and for a given value of α, increases when κ decreases. This means that an ionic liquid IPT will tend to have a larger total amount of charge transferred for a given applied voltage in comparison with a water-based IPT, which is represented by $\alpha = 0$. In Fig. 5, it is seen that the initial capacitance as $y \to 0$ varies for different values of α, but stays the same for different κ. For certain ranges of α and κ the capacitance-voltage curve becomes nonmonotonic, i.e., there is an initial increase in capacitance followed by a decrease. Whether or not the capacitance-voltage relationship is monotonic depends on the values of both α and κ. As $\kappa \to 0$ the ionic liquid ions are treated as point

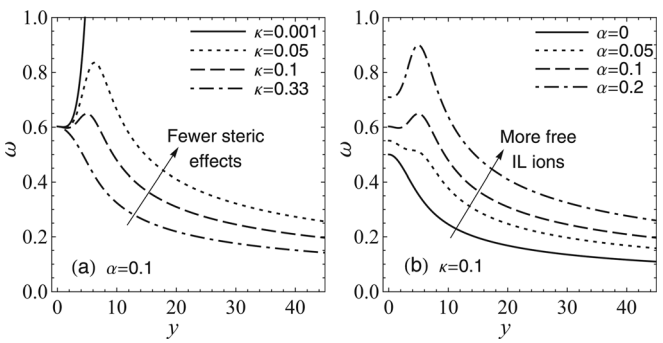

FIG. 5. Nondimensional differential capacitance for (a) a free ionic liquid fraction of $\alpha = 0.1$ with different values of the ionic liquid ion packing parameter, κ, and (b) $\kappa = 0.1$ and different values of α.

charges and steric effects are neglected. Figures 4(a) and 5(a) show that $\kappa \to 0$ leads to unreasonable predictions in charge transferred when $\alpha > 0$; it is therefore essential to include steric effects in a model of the electric double layer in ionic liquid IPTs. For all values of α with $\kappa > 0$, the capacitance always goes to zero as the total potential drop over the boundary layers, y, increases: $\lim_{y\to\infty} \omega = 0$. This means that the capacitance always continues to decrease with the applied voltage after any initial increase, eventually reaching a point where increasing the applied voltage results in zero additional charge transferred. However, this point is reached well outside of the electrolysis limit of the ionic liquid.

As an example of the decreasing differential capacitance, consider the case of $\alpha = \kappa = 0.1$. The calculated values for charge transferred for this case are shown in Table I for different applied voltages, along with a comparison of a water-based IPT, which is represented by $\alpha = 0$. From the table, it is seen that nearly as much charge accumulation occurs from 0 to 1 V as from 1 to 4 V for the ionic liquid IPT. The same result holds for the water-based IPT, which was recently analyzed by Porfiri.[39,40]

Figures 4 and 5 and Table I emphasize that the IPT is a highly nonlinear and nonideal capacitor. For an ideal capacitor, charge transferred is a linear function of the applied voltage and therefore the capacitance is constant. The voltage range where an IPT can be approximated as an ideal capacitor is very small, since the nonlinearity is seen even at low applied voltages. Ideal behavior looks to be limited to applied voltages less than the thermal voltage, i.e., $v_0 < 1$, or $V_0 < RT/F$ which is ~25 mV near room temperature. However, at lower applied voltages it may be important to also include effects of overscreening by the large ionic liquid ions for an accurate model of the electric double layer.[58] Regardless, with an ionic liquid in the system, the response becomes further from ideal, and for certain ranges of α and κ the capacitance-voltage relationship becomes nonmonotonic. These results have important implications toward actuation. Specifically, even though using an ionic liquid as solvent in an IPT will allow for higher applied voltages without electrolysis, increasing the applied voltage from, say, 1 to 2 V results in a much smaller amount of additional charge transferred than going from 0 to 1 V. This implies a reduced effectiveness in increasing the actuation response with respect to applying higher voltages to the IPT, and since ionic liquid IPT actuators are typically operated in the range of 3–4 V, this result is directly relevant for IPT actuation performance.

We also see that the fraction of free ionic liquid ions (α) and the influence of steric effects (κ) have a large impact on the shape of the capacitance-voltage curve, and determine whether or not the differential capacitance is a monotonically decreasing function of the applied voltage. In Sec. II we said that the fraction of free ionic liquid ions was unknown; indeed, this is an important question which needs to be addressed in order to accurately model the electric double in ionic liquid IPTs and understand the mechanisms of charge transport. From the results in Fig. 5, we propose that the capacitance-voltage relationship of an IPT can possibly be used to identify the extent of free ionic liquid ion movement for transducers with different ionic liquids. As mentioned in Sec. II, if the fraction of free ions was different for the ionic liquid anion and cation, this change would be a straightforward extension of the model and could be incorporated in order to make a comparison with experimental results.

TABLE I. Non-dimensional charge transferred at equilibrium for an ionic liquid IPT, q_{IL}, with $\alpha = \kappa = 0.1$ and for a water-based IPT, q_W, where $\alpha = 0$.

V_0	IL IPT (q_{IL})	Δq_{IL}	Water IPT (q_W)	Δq_w
1 V	13.65	13.65	8.25	8.25
2 V	20.10	6.45	12.00	3.75
3 V	24.97	4.87	14.85	2.85
4 V	29.04	4.07	17.24	2.39

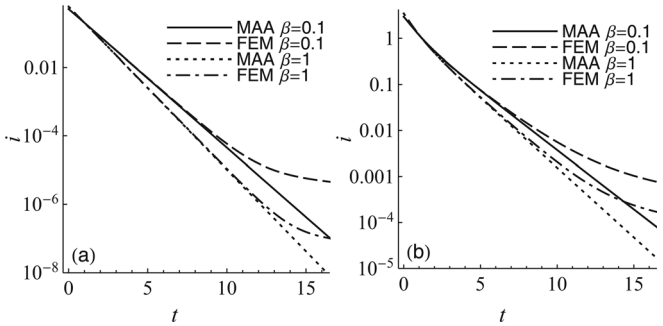

FIG. 6. Transient current in response to a step voltage of (a) $v_0 = 1$ ($V_0 \sim 25$ mV) and (b) $v_0 = 6$ ($V_0 \sim 150$ mV) for $\alpha = 0.1$ and two values of β. The numerical (FEM) results are for $\kappa = 0$, and the MAE results use the small value of $\kappa = 0.001$.

V. DYNAMIC RESPONSE

Using the results from the matched asymptotic expansion, we now look to examine the dynamic response. Specifically, we solve the governing ODE derived in Appendix A to examine the current decay in response to an applied step voltage. The MAE solution is compared to a full numerical solution for low applied voltage and the limit $\kappa \to 0$. From this comparison is it seen that the presence of nonlinear dynamics causes the MAE solution to be a poor description of current decay for $\alpha > 0$, although it has previously been shown to yield a good correlation with numerical results for the case of $\alpha = 0$.[12,39]

At leading order, the current in the IPT is

$$i = \frac{h}{Fc_0D_1}I = \left(\frac{1}{2} + \alpha\beta\right)A(t), \tag{27}$$

where i is nondimensional and I is dimensional current, and the sign is chosen such that a positive applied voltage causes a positive current. The derivation of this equation and of the governing ODE for $A(t)$ is in Appendix A. From Eq. (27) for current and Eqs. (24) and (25) for charge transferred, it is seen that the magnitude of the current through the IPT varies inversely with the thickness, and the magnitude of the charge transferred varies inversely with the Debye length.

The solution of Eq. (A4) to obtain the current via Eq. (27) is plotted in Fig. 6 for two different applied step voltages. A numerical solution of Eq. (20) for ξ^+ was used to generate

these results. Figure 6 shows results for the applied voltages $v_0 = (1, 6)$, which correspond to $V_0 \approx (25, 150)$ mV near room temperature. The parameter values used here are $\alpha = 0.1$, $\beta = (0.1, 1)$, and $\kappa = 0.001$, with the latter chosen to represent the limit as $\kappa \to 0$ and thus to correspond to classic NPP theory, i.e., neglecting steric effects.

These results are compared to numerical results generated using the method in our previous work, where steric effects were not included in the model.[12] In Ref. 12 an applied voltage of $V_0 = 150$ mV was considered, and the results in this voltage range were found to be reasonable even without the inclusion of steric effects; results for this applied voltage are shown in Fig. 6(b). The boundary layer size in the numerical results shown in Fig. 6 was defined so that $\delta = 10^{-5}$. These results show that at short times, even for different relative diffusion coefficients of the ionic liquid ions (β), the results from the matched asymptotic expansion (MAE) are in excellent agreement with the finite element method (FEM) solution. However, at long times, the two solutions deviate, with the FEM solution showing a very slow current decay while the MAE current continues to decay exponentially. This difference is entirely due to the nonlinear dynamics and the presence of the diffusive time scale, which will always exist for $\alpha > 0$; nonlinear boundary layer charging dynamics in ionic liquid IPTs are discussed in Ref. 12. The reason for attributing this difference solely to the nonlinear dynamics is clear when considering the case $\beta = 1$; here, all the ions are given the same diffusion coefficient, so there must be a physical phenomenon (the nonlinear dynamics) which is accounted for in the FEM, but not the MAE, results.

The reason for this difference in results comes from the MAE solution procedure of matching between inner and outer solutions in the limit as $\delta \to 0$. This essentially excludes nonlinear dynamics since in this limit the boundary layers are always in equilibrium with the bulk region. As discussed in Ref. 12 in regards to ionic liquid IPTs, the nonlinear dynamics occur when large amounts of ion adsorption in the boundary layers cause a local depleted region which then fills in via diffusion. (These effects are discussed in detail by Bazant *et al.*[50] and Kilic *et al.*[21] in regards to a binary electrolyte system). Diffusion is represented by the dominant time scale $\tau_d = h^2/D_1$, and indeed we see that $\tau_c/\tau_d = \lambda/h = \delta$. For the FEM results, $\delta \ll 1$ is satisfied, but δ is still nonzero. The diffusive time scale τ_d therefore causes the nonlinear dynamic response and the slow current decay at long times shown in the FEM solutions in Fig. 6. A value of $\delta = 10^{-5}$ is a reasonable choice for an IPT actuator, as can be seen from the following example. Using Eq. (6) with $\varepsilon = 10\varepsilon_0$ (EMI-Tf ionic liquid, Nafion, free water, and bound water have relative permittivities of 15.1, 3, 78, and ~7.5, respectively,[42,59,60] so this is a reasonable choice) and $C_0 = 1150$ mol/ m^3 (see Appendix C of Ref. 12) yields $\lambda = 1.5$ Å. For an IPT actuator with a total thickness of $2h = 30$ μm, we have $\lambda/h = 10^{-5}$. A reasonable range may therefore be set as $10^{-6} < \delta < 10^{-5}$. This means that the nonlinear dynamic response is expected to contribute to the current decay at long times in typical IPT actuator systems (the extent of the nonlinear dynamics increases with the applied voltage and when $\beta \ll 1$), although there are other considerations which also affect the dynamic response. The fractal-like structure of the interpenetrating electrodes will impact the charging dynamics, typically causing the current decay to follow a stretched-exponential form.[41,61–70] The porous nature of Nafion may also lead to a stretched exponential response.[71] Additionally, surface transport, which is neglected in formulating the 1D model here, is also expected to make a significant contribution to the nonlinear dynamics of an IPT, since the electrodes are far from uniform and large voltage are applied.[72]

However, since $\tau_c/\tau_d = \delta \ll 1$, we can expect that the response at short times is well approximated by $\delta \to 0$ (i.e., by the MAE results), and this is exactly what is seen in Fig. 6. Even for $\beta \neq 1$, when both the timescales τ_c and τ_c/β are present, Fig. 6 shows that the MAE results are still a good description of the current decay at short times. We can contrast this comparison with that of the MAE and FEM results for the case of $\alpha = 0$, which was shown in our previous work[12] as well as by Porfiri.[39] For $\alpha = 0$, the MAE and FEM results are in excellent agreement at all times because there are no nonlinear dynamics when $\alpha = 0$. For $\alpha > 0$, there will always be nonlinear dynamics and the MAE solution becomes a definite approximation to the transient response. Although limits for weakly and strong nonlinear dynamics are derived in Refs. 50 and 51 for a typical binary electrolyte solution, these limits are not directly applicable here due to the asymmetry of the present problem. However, we can see from Fig. 6 and from the fact that $\tau_c/\tau_d = \delta \ll 1$ that the approximation of linear dynamics leads to a good description of current decay at short times, especially for low applied voltages [for example, the MAE results have only deviated from the FEM results by 5% at $t = 6$ for the case of $\beta = 0.1$ and $v_0 = 6$ shown in Fig. 6(b)]. At higher applied voltages, the approximation will fail at shorter times, but it can reasonably be expected that the linear dynamics will continue to be a good approximation to current decay for $t < 1$ (i.e., for times less than the charging time).

Due to the nonlinear capacitance and the presence of multiple time scales, it is suggested that to characterize the capacitance by representing the IPMC as an RC circuit it is necessary to either use an applied voltage less than the thermal voltage when looking at the step response (as was done by Aureli *et al.*[41]), or a sufficiently high frequency such that the boundary layers never have time to fully form (i.e., y does not change much) when looking at the impedance response. The argument is mostly heuristic, but we can say that since the charging time scale τ_c is on the order of milliseconds,[12,41] a frequency on the order of kHz should be used as a minimum in characterizing the impedance response. Although the measurements were performed for neat ionic liquids (not ionic liquid in an ionomer), Lockett *et al.*[73] found that a frequency of 1 kHz could be used to obtain a satisfactory correlation with the full impedance results when measuring the capacitance-voltage relationship of different imidazolium-based ionic liquids. This agreement may be due to the fact that the current is large at this frequency and therefore there is not enough time for y to change a large amount in magnitude with the applied sine wave. Therefore an RC circuit is a decent approximation at this frequency (specifically a constant-phase element (CPE), not a

capacitor, is a better representation when used in series with a resistor to model the electric double layer; see, for example, Ref. 34). Olesen *et al.*[74] discuss some of these issues regarding the nonlinear response of an electrochemical system, including steric effects, to the application of an AC voltage.

From the discussion and comparison to numerical results in this section, it is seen that the MAE solutions obtained here for the dynamic current decay in response to an applied step voltage are quite limited, only applying approximately to unelectroded samples at low applied voltages and short times. This is in contrast to results considering a single mobile ionic species, where the absence of nonlinear dynamics causes the MAE results to be applicable at all times for all reasonable applied voltages. However, since the capacitance and charge transferred refer to equilibrium configurations, they are always valid, regardless of β and v_0. Capacitance and charge transferred are calculated per unit surface area. This unit surface area can be taken to be the microscopic surface area as long as the Debye length is much smaller than the microscopic surface roughness.[40] Therefore, Eqs. (25) and (26) for charge transferred and capacitance are valid for fully electroded IPTs if the boost in capacitance due to the large microscopic surface area is accounted for.

VI. IONIC CONCENTRATION AND CHARGE DENSITY

Since at leading order the boundary layers are in a state of quasiequilibrium with the bulk region, the ionic concentration profiles can be determined for a given value of y. As discussed in the previous section, these concentration profiles are valid at equilibrium, and valid transiently when there are only linear dynamics. The approximation of linear dynamics is limited to small v_0 and short times when considering a step voltage. By just considering the equilibrium distributions, however, we can see how the inclusion of steric effects impacts boundary layer composition and can obtain concentration profiles that are valid for higher applied voltages that those obtained in Ref. 12, where steric effects for the ionic liquid ions were omitted.

To calculate ionic concentration, first define $f(\hat{z}^{\pm}) = \mp\partial\hat{z}/\partial\eta$ and use Eq. (17) to express this solely in terms of the leading order expression for boundary layer potential, $\hat{z}^{(0)}$. The sign of the square root from using Eq. (17) is determined so that $f(\hat{z}^{\pm})$ is positive at the negative electrode, which is associated with $\hat{z}^{-}$, and vice versa. This can be integrated to determine η as a function of $\hat{z}$:

$$\eta^{\pm}(\hat{z}^{\pm}) = \pm\int_{\hat{z}^{\pm}(0)}^{\hat{z}^{\pm}} \frac{d\hat{z}^{\pm}}{f(\hat{z}^{\pm})}. \tag{28}$$

This gives an implicit expression for potential as a function of the inner coordinates which can be tabulated numerically. The ionic concentrations as a function of position are then be determined using Eq. (14).

Boundary layer concentration profiles for $\alpha = \kappa = 0.1$ and different values of the total potential drop across the boundary layers, y, are shown in Fig. 7 for the different ionic species. These plots show the basic behavior that the cations move toward the cathode and anion toward the anode, and that there will be a depleted region at the electrode opposite these. The concentration of the ionic liquid ions has a maximum of $2/\kappa$, and the anion reaches this concentration value at the anode for $y = 10$ and higher. Not as many ionic liquid cations move toward the cathode as anions move toward the anode because of the mobile counter-cation, and the ionic liquid cation does not reach the maximum possible concentration of $2/\kappa$ even for $y = 40$ (which is $\sim$1 V near room temperature). The concentration of the counter-cation is exponentially increasing at the cathode, and the maximum concentration at the electrode is listed in Fig. 7(a) for each value of y.

In Fig. 7 it appears as if conservation of mass for each ionic species is not enforced. However, this is actually not the case. For large applied voltages there will be neutral salt absorption by the double layer,[21] and this will cause a slight depletion in concentration in the bulk region. The charge density in the bulk region will still remain zero. In the limit

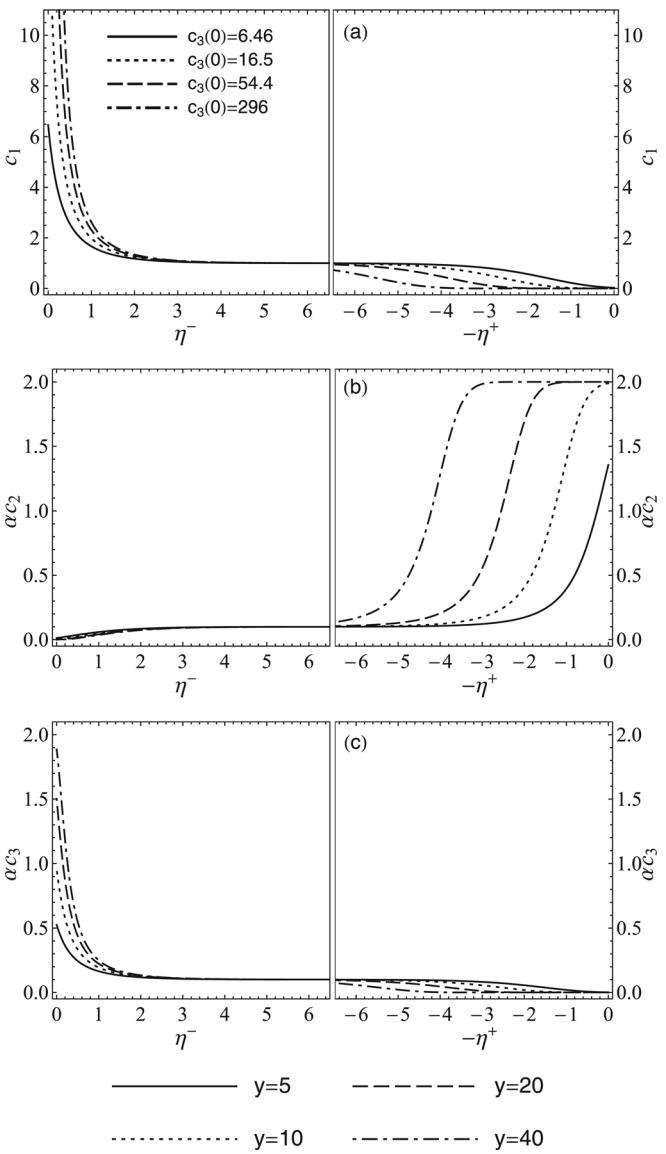

FIG. 7. Boundary layer concentration profiles for $\alpha = \kappa = 0.1$ and different values of the total potential drop across the boundary layers, y, showing (a) the counter-cation, (b) the ionic liquid anion, and (c) the ionic liquid cation. The concentration of the counter-cation at the cathode is listed in (a) for each value of y.

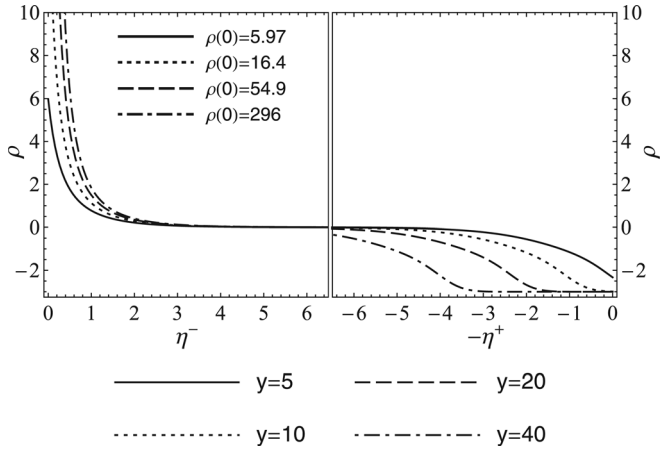

FIG. 8. Boundary layer charge density profile for $\alpha = \kappa = 0.1$ and different values of the total potential drop across the boundary layers.

of thin boundary layers, the approximation $c_i(\text{bulk}) \sim 1$ still holds, although $c_i(\text{bulk})$ will actually be slightly less than 1. A value of $c_i(\text{bulk}) < 1$ is associated with the nonlinear dynamics discussed in the previous section.

With the ionic concentration profiles, the charge density, ρ, is a simple calculation. The charge density for the same parameter values, $\alpha = \kappa = 0.1$, is shown in Fig. 8. The different characteristics of each boundary layer can easily be seen in the plot of charge density. The anode boundary layer (ABL) is much larger than the cathode boundary layer (CBL), and its size increases with the applied voltage. Since a large amount of the small counter-cations move into the CBL, its size is only slightly dependent on the applied voltage. When steric effects are omitted, the size of the CBL is not dependent on the applied voltage, and its size is characterized solely by the Debye length. Since we took α to be small, this is still the dominant trend seen in Figs. 7 and 8.

The ABL in an ionic liquid IPT is distinctly different from the ABL in a water-based IPT, as was also discussed in Ref. 12. In comparison with the results in Ref. 12, here the ABL does not have a region of increasingly negative charge density because steric effects are included. This is a more accurate description of the electric double layer at higher applied voltages considering the large sizes of the ionic liquid ions. The charge density will be −1 in the ABL of a water-based IPT but will reach $-1 - 2\alpha/\kappa$ in an ionic liquid IPT. The CBL is similar for water-based and ionic liquid IPTs in terms of size and charge density, but the charge density in the CBL for a given applied voltage will be higher for the ionic liquid IPT, where $\alpha > 0$, versus the water-based IPT, where $\alpha = 0$.

VII. DISCUSSION

A. Charging characteristics

Figure 5 shows that the ionic liquid IPT is a nonlinear capacitor, with the capacitance generally a decreasing function of the applied voltage. For large values of α or small values of κ the capacitance-voltage relationship is nonmonotonic: there is an initial increase in capacitance followed by a decrease. For a neat ionic liquid, the use of the MNPP equations yields nonmonotonic capacitance-voltage curves for $\kappa < 1/3$.[24] The ionic liquid IPT converges to follow this behavior as α increases; however, for small α, smaller values of κ are needed for ionic liquid IPT versus a neat ionic liquid for the capacitance-voltage curve to be nonmonotonic. Since $\alpha = \kappa$ is a reasonable choice for parameter values as discussed in Sec. IV, it may be expected that an ionic liquid IPT will typically feature a nonmonotonic capacitance-voltage curve. However, since many factors can influence the correct values of α and κ, a firm conclusion is best reached through a comparison with experimental results. The capacitance-voltage relationship has not been measured for ionic liquid IPTs, and this sort of an experimental model verification should be the subject of future work. Kim and Kim[75] report a capacitance-voltage measurement for a water-based IPT but did not analyze whether their results were affected by assumptions of electrode structure. As mentioned in Sec. IV, we suggest that measurements of capacitance-voltage for ionic liquid IPTs can possibly be used to identify the extent of free ionic liquid ion movement for IPTs with different ionic liquids. Newly developed experimental techniques such as neutron imaging[76] and fluorescence spectroscopy[77] may also prove useful for identifying the extent of free ionic liquid ion movement.

Figures 4 and 5 show that the presence of free ionic liquid ions will tend to increase the overall amount of charge transferred in response to an applied voltage. Therefore, to maximize the capacitance of an ionic liquid IPT, an ionic liquid should be used where a large fraction of the ions exist as free. The influence of steric effects, which is described by the parameter κ, also has a large effect on the capacitance and charge transferred. However, since the ionic liquid exists in the polymer, not as a neat solution, the correct value of κ will be different from that for a neat solution. Again, a comparison of experimentally measured capacitance-voltage curves for an ionic liquid IPT with those predicted by Eq. 26 could give insight as to the correct values of α and κ to use to describe an actuator system.

We also saw that although the capacitance, charge transferred, and equilibrium ionic concentration profiles are well described by the results of the matched asymptotic expansion, the dynamic response is not. This is in contrast to the water-based IPT with $\alpha = 0$, where there are no nonlinear dynamics and the results of the matched asymptotic expansion show an excellent agreement with numerical results at all times.[12,39] In Sec. V we showed that nonlinear dynamics and the presence of multiple times scales causes the calculated current from the matched asymptotic expansion to only be a good approximation at short times and small applied voltages. The electrode structure and porous nature of the ionomer will also affect the dynamic response; these are additional factors which need to be considered in comparing the theoretical results here with experiment.

B. Actuation performance

Although the presence of free ionic liquid ions will tend to increase the total amount of charge transferred, this does not necessarily mean it will increase the actuation response in

bending of a transducer. As discussed in Ref. 9, where a micromechanics model is applied to model the actuation of ionic liquid IPTs, the mobile ionic liquid ions can affect the actuation response in bending by both finite size effects and from changes in boundary layers stress caused by changes in charge density. The physical mechanisms responsible for the coupling between changes in charge density and the stress developed in the boundary layers are, in general, quite complicated; modeling these processes is currently the subject of research (see, for example, Refs. 9, 29, and 37). However, using the results of Sec. VI, the influence of ionic liquid ions on the actuation response of IPTs can be assessed. Figure 7 shows the ionic concentrations in the boundary layers for the parameter values $\alpha = \kappa = 0.1$ and for different values of the total potential drop across the boundary layers, which is equal to the applied voltage at equilibrium. These plots show that the counter-cation is still by far the dominant charge carrier, with large amounts accumulating at the cathode. For the ionic liquid ions, although it was specified that the same number of free positive and negative ions exist, the concentration distributions are quite asymmetric. The amount of ionic liquid anions moving into the anode boundary layer (ABL) is much larger than the amount of ionic liquid cations moving into the cathode boundary layer (CBL). However, the presence of a mobile anion also increases the amount of counter-cations moving into the CBL. Since an increase in charge density in the ABL makes a negative contribution to the overall bending moment of the actuator, the extra charge transferred due to the presence of the mobile ionic liquid ions may not increase the overall bending actuation response of the IPT. This suggests that the maximum electromechanical conversion efficiency for bending movement of an ionic liquid IPT actuator will occur when $\alpha = 0$, i.e., the case with the largest asymmetry in the charge distribution. In practice, this may correspond to using an ionic liquid where the ions are more tightly bound and do not dissociate as easily when swollen in Nafion. Since it is the asymmetry in the charge density distribution that drives bending actuation, a similar performance increase to using an ionic liquid with $\alpha = 0$ may be achieved by using an ionic liquid where the anion is relatively immobile compared to the cation. These conclusions are the same as were reached in our previous work,[12] where they were discussed in more depth, and have been qualitatively shown to be in agreement with recent experimental results.[7] Here, our solutions are valid for higher applied voltages, although for $V_0 \sim 1$ V Fig. 7(a) shows that MNPP theory might also be needed for the counter-cation since a high concentration value is obtained. With the present analysis the inclusion of steric effects leads to a realistic description of boundary layer composition at voltages near IPT operating voltages.

VIII. CONCLUSIONS

Using a modified Nernst-Planck equation to account for steric effects in movement of the large ionic liquid ions, we analyzed the charging characteristics of ionic liquid IPTs by considering both the anion and cation of the ionic liquid in addition to the counter-cation as mobile ionic species. Analytical expressions for the charge transferred and capacitance as functions of the applied voltage, free ionic liquid fraction α, and packing parameter κ were derived using the method of matched asymptotic expansions. The results show distinct differences in charge transfer characteristics in ionic liquid IPTs versus their water-based counterparts: for a given applied voltage, the presence of free ionic liquid ions causes an increase in the overall amount of charge transferred. However, the decreasing differential capacitance translates into marginally less charge transferred as the applied voltage is increased. A governing ODE for the dynamic charging response was derived using the results of the matched asymptotic expansion, and the leading order relationship for charge stored in the boundary layers with respect to time (i.e., current) was established. Although it was shown that at leading order the charge stored in the boundary layers is determined solely by the total potential drop across the boundary layers (y), a comparison with numerical results demonstrated that the leading order dynamics are only a good description for short times and small applied voltages. The solution here using the method of matched asymptotic expansions does not capture the multiple time scales and nonlinear dynamic response discussed in Ref. 12. Therefore, although the results of the matched asymptotic expansion are a good description of capacitance and charge transferred with respect to the applied voltage and of the equilibrium ionic concentration profiles, a full description of the dynamic response requires a numerical solution or an alternate solution procedure. The distributions for boundary layer ionic concentration and charge density were obtained numerically and used to explain the actuation characteristics of ionic liquid IPTs in comparison with water-based IPTs. Specifically, although an ionic liquid IPT will have more charge transferred that an identical water-based IPT, the increased charge density in the anode boundary layer will make a negative contribution to the overall bending moment. This suggests that to maximize electromechanical conversion efficiency in bending actuation, an ionic liquid with a small fraction of free ions should be used, and to maximize the overall charge transferred, an ionic liquid with a large fraction of free ions should be used. Measurements of the capacitance-voltage relationship for ionic liquid IPTs in comparison with the theoretical result of Eq. (26) can possibly be used to identify the extent of free ionic liquid ion movement for ionic liquid IPTs with different ionic liquids.

ACKNOWLEDGMENTS

This work was supported in part by the U.S. Army Research Office under Grant No W911NF-07-1-0452 Ionic Liquids in W911NF-07-1-0452 Ionic Liquids in Electro-Active Devices (ILEAD) MURI.

APPENDIX A: GOVERNING EQUATIONS FOR LEADING ORDER CURRENT RESPONSE

To derive the governing ODE for $A(t)$ [recall that current is related to $A(t)$ by Eq. (27)], begin by considering the total diffuse charge stored from the electrode to a point η in the double layer. This can be expressed using the inner coordinates as

$$q(\eta) = \int_0^{\eta} (\hat{c}_1 - \alpha\hat{c}_2 + \alpha\hat{c}_3 - 1)d\eta, \tag{A1}$$

where the quantity in parenthesis is the charge density. Differentiating with respect to time and using Eq. (10), this becomes

$$\frac{dq(\eta)}{dt} = -\frac{1}{\delta}(\hat{j}_1 - \alpha\hat{j}_2 + \alpha\hat{j}_3), \tag{A2}$$

where $\hat{j}_i$ are the fluxes of the ions. We now match the inner and outer solutions in the limit of thin boundary layers as in Sec. III. This yields

$$\begin{aligned}\lim_{\eta^{\pm}\to\infty} \frac{dq(\eta)}{dt} &= \lim_{\eta\to\infty} -\frac{1}{\delta}(\hat{j}_1 - \alpha\hat{j}_2 + \alpha\hat{j}_3) \\ &= \lim_{x\to\pm 1} -(\bar{j}_1 - \alpha\bar{j}_2 + \alpha\bar{j}_3) \\ &= \mp\left(\frac{1}{2} + \alpha\beta\right) A(t),\end{aligned} \tag{A3}$$

where Eqs. (7), (9a), and (10) are used. Positive charge accumulates in the cathode boundary layer, which is modeled with η^-, and negative charge accumulates in the anode boundary layer, which is modeled with η^+. As $\eta \to \infty$ in the integral of Eq. (A1), the calculated charge transferred represents the total charge in the double layer. Therefore, Eq. (A3) leads to Eq. (27) for the transient current in the membrane.

To determine the governing ODE for $A(t)$, recall that the charge transferred is known from Eq. (25). Using this, we have a governing first-order nonlinear ODE for $A(t)$ which can be evaluated numerically:

$$\frac{\partial q}{\partial y}\frac{\partial y}{\partial t} = \left(\frac{1}{2} + \alpha\beta\right) A(t), \tag{A4}$$

where $\partial q/\partial y = \omega$ is given in Eq. (26). The initial condition will vary depending on the nature of the applied voltage. For a step voltage applied at $t = 0$, the initial condition is $A(0) = v_0$ since the zeta potential will initially be zero at the instant when the voltage is first applied.

[1] M. D. Bennett, *Electromechanical Transduction in Ionic Liquid-Swollen Nafion Membranes*, Ph.D. thesis, Virginia Tech, 2005.
[2] M. D. Bennett and D. J. Leo, Sens. Actuators A: Phys. **115**, 79 (2004).
[3] B. J. Akle, M. D. Bennett, and D. J. Leo, Sens. Actuators A **126**, 173 (2006).
[4] J. Wang, C. Xu, M. Taya, and Y. Kuga, Smart Mater. Struct. **16**, S214 (2007).
[5] K. Kikuchi and S. Tsuchitani, J. Appl. Phys. **106**, 053519 (2009).
[6] J. Lee and Y. Yoo, Sens. Actuators B **137**, 539 (2009).
[7] S. Liu, W. Liu, Y. Liu, J. Lin, X. Zhou, M. J. Janik, R. H. Colby, and Q. Zhang, Polym. Int. **59**, 321 (2010).
[8] Y. Liu, S. Liu, J. Lin, D. Wang, V. Jain, R. Montazami, J. Heflin, J. Li, L. Madsen, and Q. Zhang, Appl. Phys. Lett. **96**, 223503 (2010).
[9] J. D. Davidson, *Actuation and Charge Transport Modeling of Ionic Liquid-Ionic Polymer Transducers*, Master's thesis, Virginia Tech, 2010.
[10] M. Armand, F. Endres, D. R. MacFarlane, H. Ohno, and B. Scrosati, Nat. Mater. **8**, 621 (2009).
[11] W. Lu, A. G. Fadeev, B. Qi, E. Smela, B. R. Mattes, J. Ding, G. M. Spinks, J. Mazurkiewicz, D. Zhou, G. G. Wallace, D. R. MacFarlane, S. A. Forsyth, and M. Forsyth, Science **297**, 983 (2002).
[12] J. D. Davidson and N. C. Goulbourne, J. Appl. Phys. **109**, 014909 (2011).
[13] J. J. Bikerman, Philos. Mag. Ser. **7**, 384 (1942).
[14] M. Dutta and M. Sengupta, in *Proceedings of the National Institute of Sciences of India*, Vol. **20** (National Institute of Sciences of India, Calcutta, India, 1954) p. 1–11.
[15] M. Eigen and E. Wicke, J. Phys. Chem. **58**, 702 (1954).
[16] P. Strating and F. W. Wiegel, J. Phys. A **26**, 3383 (1993).
[17] V. Kralj-Iglic and A. S. Igli, Electrotech. Rev. **61**, 127 (1994).
[18] I. Borukhov, D. Andelman, and H. Orland, Phys. Rev. Lett. **79**, 435 (1997).
[19] I. Borukhov, D. Andelman, and H. Orland, Electrochim. Acta **46**, 221 (2000).
[20] K. Bohinc, V. Kralj-Iglic, and A. Iglic, Electrochim. Acta **46**, 3033 (2001).
[21] M. S. Kilic, M. Z. Bazant, and A. Ajdari, Phys. Rev. E **75**, 021503 (2007).
[22] M. S. Kilic, M. Z. Bazant, and A. Ajdari, Phys. Rev. E **75**, 021502 (2007).
[23] M. Z. Bazant, M. S. Kilic, B. D. Storey, and A. Ajdari, Adv. Colloid Interface Sci. **152**, 48 (2009).
[24] A. A. Kornyshev, J. Phys. Chem. B **111**, 5545 (2007).
[25] K. B. Oldham, J. Electroanal. Chem. **613**, 131 (2008).
[26] M. V. Fedorov and A. A. Kornyshev, J. Phys. Chem. B **112**, 11868 (2008).
[27] M. V. Fedorov and A. A. Kornyshev, Electrochim. Acta **53**, 6835 (2008).
[28] M. Shahinpoor, Electrochim. Acta **48**, 2343 (2003).
[29] S. Nemat-Nasser, J. Appl. Phys. **92**, 2899 (2002).
[30] B. J. Akle, D. J. Leo, M. A. Hickner, and J. E. McGrath, J. Mater. Sci. 40, 3715 (2005).
[31] R. A. Robinson and R. H. Stokes, *Electrolyte Solutions*, 2nd ed. (Butterworths Publications Limited, London, 1959).
[32] J. Bockris and A. Reddy, *Modern Electrochemistry 1* (Plenum Press, New York, 1998).
[33] J. M. G. Barthel, H. Krienke, and W. Kunz, *Physical Chemistry of Electrolyte Solutions*, Vol. **5** (Springer, New York, 1998).
[34] A. J. Bard and L. R. Faulkner, *Electrochemical Methods: Fundamentals and Applications*, 2nd ed. (Wiley, New York, 2000).
[35] T. Wallmersperger, B. J. Akle, D. J. Leo, and B. Kröplin, Compos. Sci. Technol. **68**, 1173 (2008).
[36] T. Wallmersperger, A. Horstmann, B. Kröplin, and D. J. Leo, Journal of Intelligent Material Systems and Structures, **20**, 741 (2009).
[37] T. Wallmersperger, D. J. Leo, and C. S. Kothera, J. Appl. Phys. **101**, 024912 (2007).
[38] D. J. Leo, K. Farinholt, T. Wallmersperger, and Y. Bar-Cohen, in *Smart Structures and Materials 2005: Electroactive Polymer Actuators and Devices (EAPAD)*, Vol. **5759** (SPIE, San Diego, CA, USA, 2005) pp. 170–181.
[39] M. Porfiri, J. Appl. Phys. **104**, 104915 (2008).
[40] M. Porfiri, Phys. Rev. E **79**, 041503 (2009).
[41] M. Aureli, W. Lin, and M. Porfiri, J. Appl. Phys. **105**, 104911 (2009).
[42] M. Porfiri, Smart Mater. Struct. **18**, 015016 (2009).
[43] Z. Chen, D. R. Hedgepeth, and X. Tan, Smart Mater. Struct. **18**, 055008 (2009).
[44] K. M. Newbury and D. J. Leo, J. Intell. Mater. Syst. Struct. **14**, 333 (2003).
[45] J. W. Paquette, K. J. Kim, J. Nam, and Y. S. Tak, J. Intell. Mater. Syst. Struct. **14**, 633 (2003).
[46] P. J. Branco and J. A. Dente, Smart Mater. Struct. **15**, 378 (2006).
[47] C. Bonomo, L. Fortuna, P. Giannone, S. Graziani, and S. Strazzeri, Smart Mater. Struct. **16**, 1 (2007).
[48] K. M. Farinholt and D. J. Leo, J. Appl. Phys. **104**, 014512 (2008).
[49] A. Punning, U. Johanson, M. Anton, A. Aabloo, and M. Kruusmaa, J. Intell. Mater. Syst. Struct. **20**, 1711 (2009).
[50] M. Z. Bazant, K. Thornton, and A. Ajdari, Phys. Rev. E **70**, 021506 (2004).
[51] J. D. Davidson and N. C. Goulbourne, Proc. SPIE **7289**, 72891F (2009).
[52] M. D. Bennett, D. J. Leo, G. L. Wilkes, F. L. Beyer, and T. W. Pechar, Polymer **47**, 6782 (2006).
[53] M. Z. Bazant, K. T. Chu, and B. J. Bayly, SIAM J. Appl. Math. **65**, 1463 (2005).
[54] V. Barcilon, D. Chen, R. S. Eisenberg, and J. W. Jerome, SIAM J. Appl. Math. **57**, 631 (1997).
[55] G. Richardson and J. King, J. Eng. Math. **59**, 239 (2007).
[56] For a practical size comparison, the effective radii of EMI+ and Tf- are calculated to be 3.3 Å and 2.5 Å, respectively, using the effective molecular volume determined from the ab initio calculations in Ref. 7.
[57] J. D. Davidson and N. C. Goulbourne, in *Electroactive Polymer Actuators and Devices (EAPAD) 2*, Vol. **7642**, edited by Y. Bar-Cohen (SPIE, San Diego, CA, USA, 2010) pp. 76421L-14.

[58]M. Z. Bazant, B. D. Storey, and A. A. Kornyshev, Phys. Rev. Lett. **106**, 46102 (2011).
[59]H. Weingartner, Z. Phys. Chem. **220**, 1395 (2006).
[60]I. Danielewicz-Ferchmin, J. Phys. Chem. **99**, 5658 (1995).
[61]Y. Feldman, E. Polygalov, I. Ermolina, Y. Polevaya, and B. Tsentsiper, Meas. Sci. Technol. **12**, 1355 (2001).
[62]T. C. Halsey and M. Leibig, Phys. Rev. A **43**, 7087 (1991).
[63]T. C. Halsey and M. Leibig, Ann. Phys. **219**, 109 (1992).
[64]R. Kant and S. K. Rangarajan, J. Electroanal. Chem. **552**, 141 (2003).
[65]E. K. Lenzi, L. R. Evangelista, and G. Barbero, J. Phys. Chem. B **113**, 11371 (2009).
[66]T. Pajkossy and L. Nyikos, Phys. Rev. B **42**, 709 (1990).
[67]H. Sakaguchi and R. Baba, Phys. Rev. E **75**, 051502 (2007).
[68]H. Sanabria, Phys. Rev. E **74**, 051505 (2006).
[69]B. Sapoval, *Fractals and Disordered Systems*, 2nd ed., edited by A. Bunde and S. Havlin, (Springer, New York, 1996) pp. 232–261.
[70]T. Pajkossy, J. Electroanal. Chem. **364**, 111 (1994).
[71]H. Sakaguchi and R. Baba, Phys. Rev. E **76**, 011501 (2007).
[72]K. T. Chu and M. Z. Bazant, Phys. Rev. E **74**, 011501 (2006).
[73]V. Lockett, R. Sedev, J. Ralston, M. Horne, and T. Rodopoulos, J. Phys. Chem. C **112**, 7486 (2008).
[74]L. H. Olesen, M. Z. Bazant, and H. Bruus, Phys. Rev. E **82**, 011501 (2010).
[75]D. Kim and K. J. Kim, J. Intell. Mater. Syst. Struct. 449 (2006).
[76]J. K. Park, P. J. Jones, C. Sahagun, K. A. Page, D. S. Hussey, D. L. Jacobson, S. E. Morgan, and R. B. Moore, Soft Matter **6**, 1444 (2010).
[77]I. Park, S. Kim, D. Pugal, L. Huang, S. Tam-Chang, and K. J. Kim, Appl. Phys. Lett. **96**, 043301 (2010).